Improved global estimations of gross primary productivity of natural vegetation types by incorporating plant functional type

Lin, Shangrong ; Li, Jing ; Liu, Qinhuo ; Gioli, Beniamino ; Paul-Limoges, Eugénie ; Buchmann, Nina ; Gharun, Mana ; Hörtnagl, Lukas ; Foltýnová, Lenka ; Dusek, Jiri ; Li, Longhui ; Yuan, Wenping

Abstract: Satellite-based light use efficiency (LUE) models are important tools for estimating regional and global vegetation gross primary productivity (GPP). However, all LUE models assume a constant value of maximum LUE at canopy scale (LUEmaxcanopy) over a given vegetation type. This assumption is not supported by observed plant traits regulating LUEmaxcanopy, which varies greatly even within the same ecosystem type. In this study, we developed an improved satellite data driven GPP model by identifying the potential maximal GPP (GPPPOT) and their dominant climate control factor in various plant functional types (PFT), which takes into account both plant trait and climatic control inter-dependence. We selected 161 sites from the FLUXNET2015 dataset with eddy covariance CO2 flux data and continuous meteorology to derive GPPPOT and their dominant climate control factor of vegetation growth for 42 natural PFTs. Results showed that (1) under the same phenology and incident photosynthetic active radiation, the maximal variance of GPPPOT is found in different PFTs of forests (10.9 g C m−2 day−1) and in different climatic zones of grasslands (>10 g C m−2 day−1); (2) intra-annual change of GPP in tropical and arid climate zones is mostly driven by vapor pressure deficit (VPD) changes, while temperature is the dominant climate control factor in temperate, boreal and polar climate zones; even under the same climate condition, physiological stress in photosynthesis is different across PFTs; (3) the model that takes into account the plant trait difference across PFTs had a higher agreement with flux tower-based GPP data (GPPflux) than the GPP products that omit PFT differences. Such agreement was highest for natural vegetation cover sites (R2 = 0.77, RMSE = 1.79 g C m−2 day−1). These results suggest that global scale GPP models should incorporate both plant traits and their dominant climate control factor variance in various PFT to reduce the uncertainties in terrestrial carbon assessments.

DOI: https://doi.org/10.1016/j.jag.2021.102328

Lin, Shangrong; Li, Jing; Liu, Qinhuo; Gioli, Beniamino; Paul-Limoges, Eugénie; Buchmann, Nina; Gharun, Mana; Hörtnagl, Lukas; Foltýnová, Lenka; Dusek, Jiri; Li, Longhui; Yuan, Wenping (2021). Improved global estimations of gross primary productivity of natural vegetation types by incorporating plant functional type. International Journal of Applied Earth Observation and Geoinformation, 100:102328. DOI: https://doi.org/10.1016/j.jag.2021.102328

International Journal of Applied Earth Observations and Geoinformation 100 (2021) 102328

Contents lists available at ScienceDirect

International Journal of Applied Earth Observations and Geoinformation

journal homepage: www.elsevier.com/locate/jag

Improved global estimations of gross primary productivity of natural vegetation types by incorporating plant functional type

Shangrong Lin [a,b], Jing Li [a,*], Qinhuo Liu [a], Beniamino Gioli [c], Eugenie Paul-Limoges [d], Nina Buchmann [e], Mana Gharun [e], Lukas Hörtnagl [e], Lenka Foltýnová [f], Jiří Dušek [f], Longhui Li [g,h], Wenping Yuan [b]

[a] State Key Laboratory of Remote Sensing Science, Jointly Sponsored by Aerospace Information Research Institute, Chinese Academy of Sciences and Beijing Normal University, Beijing 100101, China
[b] School of Atmospheric Sciences, Southern Marine Science and Engineering Guangdong Laboratory (Zhuhai), Sun Yat-sen University, Zhuhai 519082, Guangdong, China
[c] CNR IBE, Institute of Bioeconomy, Via Caproni 8, Firenze, Italy
[d] Department of Geography, University of Zurich, 8057 Zurich, Switzerland
[e] Department of Environmental Systems Science, Institute of Agricultural Sciences, ETH Zurich, Universitätstrasse 2, CH-8092 Zurich, Switzerland
[f] Global Change Research Institute, Czech Academy of Sciences, Bělidla 4a, 603 00 Brno, Czech Republic
[g] Jiangsu Center for Collaborative Innovation in Geographical Information Resource Development and Application, Nanjing 210023, China
[h] Ministry of Education Key Laboratory for Geographical Environment Evolution, Nanjing 210023, China

ARTICLE INFO

Keywords:
Terrestrial carbon cycle
Carbon flux
Plant trait
Climatic zones

ABSTRACT

Satellite-based light use efficiency (LUE) models are important tools for estimating regional and global vegetation gross primary productivity (GPP). However, all LUE models assume a constant value of maximum LUE at canopy scale ($LUE_{maxcanopy}$) over a given vegetation type. This assumption is not supported by observed plant traits regulating $LUE_{maxcanopy}$, which varies greatly even within the same ecosystem type. In this study, we developed an improved satellite data driven GPP model by identifying the potential maximal GPP (GPP_{POT}) and their dominant climate control factor in various plant functional types (PFT), which takes into account both plant trait and climatic control inter-dependence. We selected 161 sites from the FLUXNET2015 dataset with eddy covariance CO_2 flux data and continuous meteorology to derive GPP_{POT} and their dominant climate control factor of vegetation growth for 42 natural PFTs. Results showed that (1) under the same phenology and incident photosynthetic active radiation, the maximal variance of GPP_{POT} is found in different PFTs of forests (10.9 g C m^{-2} day^{-1}) and in different climatic zones of grasslands (>10 g C m^{-2} day^{-1}); (2) intra-annual change of GPP in tropical and arid climate zones is mostly driven by vapor pressure deficit (VPD) changes, while temperature is the dominant climate control factor in temperate, boreal and polar climate zones; even under the same climate condition, physiological stress in photosynthesis is different across PFTs; (3) the model that takes into account the plant trait difference across PFTs had a higher agreement with flux tower-based GPP data (GPP_{flux}) than the GPP products that omit PFT differences. Such agreement was highest for natural vegetation cover sites (R^2 = 0.77, RMSE = 1.79 g C m^{-2} day^{-1}). These results suggest that global scale GPP models should incorporate both plant traits and their dominant climate control factor variance in various PFT to reduce the uncertainties in terrestrial carbon assessments.

1. Introduction

Terrestrial ecosystem gross primary productivity (GPP) is a fundamental component of the global carbon cycle (Beer et al., 2010; Keenan and Williams, 2018). For regional and global assessments of GPP, remote sensing is the most effective method (Running, 2004; Ryu et al., 2019; Xiao and Hollinger, 2004b; Xiao and Zhang, 2004a). Three types of GPP models based on medium spatial resolution satellite data are available to evaluate regional to global scale carbon fluxes (Schaefer et al., 2012). (1) Statistical models, which include satellite-derived

* Corresponding author.
E-mail address: lijing01@radi.ac.cn (J. Li).

https://doi.org/10.1016/j.jag.2021.102328
Received 18 December 2020; Received in revised form 10 March 2021; Accepted 19 March 2021
Available online 10 April 2021

vegetation indices GPP models (Goward et al., 1985; Sims et al., 2008; Wu, et al., 2010; Joiner et al., 2018) or machine learning GPP models with meteorological data and remote sensing data as input (e.g. FLUXCOM GPP, (Jung et al., 2011)), were used in the first attempts at mapping GPP at the global scale. (2) Semi-empirical models, which quantify GPP as a function of light use efficiency (LUE) and absorbed photosynthetic active radiation (APAR), are highly accurate models (Running et al., 2004; Xiao, Hollinger, et al., 2004; Yuan et al., 2007; Wei et al., 2017; Zhang et al., 2017). This kind of models use a constant maximal light use efficiency coupled with climatic control factors for each vegetation type, then combine it with APAR from remote sensing data to estimate GPP; these estimates can be derived from canopy to global scale. (3) Process-based models focus on the mechanistic description of the photosynthetic biochemical processes at the leaf and canopy scale by incorporating the full theoretical basis of photosynthesis (Farquhar et al., 1980; Ryu et al., 2011). These models need specific photosynthetic trait inputs for each species and canopy structure (Chen et al., 1999). Recently, this kind of models have been coupled with remote sensing data for global-scale carbon flux assessments (Jiang and Ryu, 2016; He et al., 2018). All these models combine remote sensing data and apply different parameterization methods to simulate vegetation growth, and some of them consider the variance in plant growth response in different vegetation types.

Ecosystem GPP data from the FLUXNET CO_2 dataset have been used to evaluate the accuracy of remote sensing-based GPP models (Baldocchi et al., 2001; Turner et al., 2005, 2006). The validation results from FLUXNET showed that remote sensing-based GPP models can explain about 70% (53%~78%) of site level GPP changes (Jiang and Ryu, 2016; Joiner, 2018; Yuan et al., 2014; Zhang et al., 2017). However, there are still high GPP estimation uncertainties (root mean square error, RMSE > 2.3 g C m^{-2} day^{-1}) in forest sites (Jiang and Ryu, 2016), especially in evergreen broad leaf forests, which have very low agreement (coefficient of determination, $R^2 < 0.3$) with carbon flux data (Ryu et al., 2019; Yuan et al., 2014). A possible reason for this is that the remote sensing-based models account less for climate controls and plant trait differences across species (Kattge, 2011; Rogers, 2017; Ryu et al., 2019; Xiao, 2019). Most remote sensing driven GPP models assume that vegetation growth is subject to a similar climate stress under the same meteorological conditions across climate zones (Running, 2004; Ryu et al., 2011; Xiao and Hollinger, 2004b; Xiao and Zhang, 2004a). For example, remote sensing GPP models based on LUE only account for some key properties such as the maximum light use efficiency (LUE_{max}) of different vegetation types without considering their difference and influence to photosynthesis across species (Running et al., 2004; Xiao et al., 2004). However, the canopy scale maximal LUE ($LUE_{maxcanpoy}$) is very different across PFTs (Zhang et al., 2018). Because the canopy-scale vegetation structure varies across climate zones, the observed $LUE_{maxcanpoy}$ adjusted to maximal GPP could be very different.

Studies have highlighted that photosynthesis-related plant trait properties are very different across species and geographic zones and that GPP is a significantly influenced plant trait. Although research shows that it is possible to model GPP with a vegetation-invariant set of parameters under certain conditions (Yuan et al., 2014), other studies found that plant photosynthetic traits such as the maximum carboxylation rate (Vcmax) and the maximum electron transport rate (Jmax) can differ strongly across species and vegetation types in different geographic zones (Kattge, 2011; Luo, et al., 2019) impacting GPP. Niinemets et al. (2015) showed that Vcmax ranged from 1.64 to 176.7 umol m^{-2} s^{-1} across species and varies significantly across geographical zones. A global scale comparison shows that vegetation photosynthetic traits such as Vcmax and Jmax are much higher in the Arctic zone than in the tropical zone (Ali et al., 2015). The Vcmax of conifer species in the Mediterranean zone is almost two times higher than that in non-Mediterranean zones (Flexas et al., 2014). Thus, the same vegetation type can also have >40 umol m^{-2} s^{-1} of Vcmax difference across geographical zones because of vegetation properties (Groenendijk et al., 2011). This variance leads to high GPP estimation uncertainties.

Physiological stress due to climatic conditions in the photosynthetic process is also very different across plant species (Pappas et al., 2016; Walker et al., 2017). Environmental variables such as light, temperature, vapor pressure deficit (VPD), and soil water content have different spatial patterns across different climate zones, leading to different physiological stresses to vegetation photosynthesis across species (Ali et al., 2015; Rogers et al., 2017; Wu et al., 2017). Vegetation types, aggregated plant species into several types, also undergo major climatic stressors in different geographical zones. For example, the GPP of evergreen broadleaf forests (EBF) under hot and humid conditions (tropical zones) is controlled by the amount of incident light (Gebremichael and Barros, 2006; Wu et al., 2017) and showed low agreement ($R^2 < 0.1$) to temperature. This contrasts with the GPP of EBF in Mediterranean zones, which is driven by soil water (Garbulsky et al., 2014; Liu et al., 2015). The optimal growing temperature can differ by 5 °C in some temperate and boreal forest types (Sendall et al., 2015). Studies have also highlighted the interrelationship between different climatic factors, including temperature, VPD, and light (Dass et al., 2015). Usually, temperature and VPD are highly correlated, since VPD is computed from temperature and relative humidity (RH) (Pereira et al., 2015). PAR is also highly correlated with VPD, because an increase in PAR means less cloudiness and more direct solar radiance. When the canopy has a higher fraction of direct solar radiance, the plants also suffer more water stress under higher VPD (Brando et al., 2010). Moreover, PAR also shows a high correlation with daily temperature. Thus, under a certain incident energy and phenological condition, either temperature or VPD can represent climate stress to vegetation growth. Research shows that canopy light use efficiency-based GPP models following Liebig's law that take into account the stress of temperature and water have high estimation accuracy (Yuan et al., 2007). Therefore, under a certain incident energy and vegetation phenology period, GPP is more related to the dominant climate control of either temperature or VPD. Thus, remote sensing data driven GPP models should take into account the climate stress to photosynthesis across both species and climate zones.

The concept of plant functional types (PFT) can be used to group shared traits of many plant species into a relatively low number of classes (Reichstein et al., 2014). Compared to complex species and climate gradient conditions, PFTs reduce the complexity of ecological functions into several major types. The GPP from some earth system models discriminate how plant traits affect vegetation photosynthesis (Sitch et al., 2003) by setting different maximum carboxylation rates (Vcmax) across PFTs (Groenendijk et al., 2011; Harper, 2016; Musavi, 2016; Reichstein, et al., 2014). However, unlike in these earth system models, most remote sensing data driven GPP do not change the climate control factor across various climate zones (Sun et al., 2019). Besides, remote sensing GPP models (e.g. the MODIS-GPP algorithm, hereafter named MOD17A2) rarely take into account plant trait differences across PFTs, as they rely on a simple Biome Property Look-Up Table (BPLUT) (Running et al., 2004).

The objective of this study was to build an improved framework for estimating GPP with remote sensing data by considering the differences in both plant traits and major climate controlling factors in various PFTs. We hypothesized that separating the major plant traits of vegetation photosynthetic activity in different climate zones and vegetation types can improve the estimation accuracy of GPP. We analyzed: 1) the plant trait differences in the maximum daily GPP across PFTs; 2) the dominant climate control factors and their stress level across PFTs; 3) the correlation of the improved framework with global site-level GPP (GPP_{flux}). In addition, we applied climate and GPP_{flux} data from the FLUXNET 2015 dataset to 42 different PFTs to evaluate the role of plant traits and climate stress differences, and we compared the GPP estimates based on the improved framework and three satellite-based GPP products against GPP_{flux}.

2. Data and methods

2.1. Plant functional type classification

We represented vegetation as PFTs derived from the combination of vegetation types and climate types to classify the vegetation physiological response across climatic and vegetation type variability (Fig. 1). The International Geosphere Biosphere Programme (IGBP) land cover classification has 12 major vegetation types, including deciduous broadleaf forest (DBF), evergreen broadleaf forest (EBF), deciduous needleleaf forest (DNF), evergreen needleleaf forest (ENF), mixed forest (MF), savannah (SAV), woody savannah (WSA), open shrub (OSH), close shrub (CSH), cropland (CRO), grass (GRA), wetland (WET).

The Köppen classification divides the world land surface area into five major climate zones (Peel et al., 2007), named Tropical (A), Arid (B), Temperate (C), boreal (D), and Polar (E). Each major climate zone is divided into two to four subtypes with different humidity conditions (supplementary, Table S2). From wettest to driest, the tropical area was divided into rainforest (Ar), monsoon (Am) and woody savannah area (Aw). The arid region was separated into desert (BW) and steppe (BS) types. The temperature region was split into humid/monsoon (Cf), Mediterranean (Cs), and dry (Cw) types. Similarly, the boreal region was also divided into humid (Df), dry summer (Ds), and dry winter (Dw) types. Lastly, the polar area was divided into tundra (ET) and frost (EF) regions. Overall 62 PFTs were obtained by the combination of the IGBP vegetation types with the climate zones.

2.2. Carbon flux data and remote sensing data

Daily CO_2 flux data and ERA-interim weather data were derived from the FLUXNET2015 Dataset, which provides carbon flux and meteorological data from 2001 to 2014 (http://fluxnet.ornl.gov/). We selected 10 major vegetation types of natural vegetation cover from the IGBP, from the tropical to polar region. We only selected sites located in natural PFTs (thus excluding cropland sites) with >3 site years of data in the FLUXNET2015 Dataset. In total, in this study we used 161 sites and 1180 site years of 42 PFT (Table 1).

The GPP data were from the daytime partitioning method of net ecosystem CO_2 exchange (Lasslop et al., 2010). We aggregated the flux tower-based GPP product into 8-day intervals, to be consistent with the temporal resolution of the MOD17A2 GPP product. Both the MOD17A2 product and flux tower-based GPP were averaged over daily intervals. We excluded GPP data when the mean 8-days aggregated quality flag (QC), named NEE_VUT_REF_QC, was less than 0.8. Air temperature (T) and VPD of the 8-day intervals were aggregated as the average value over 8 days with 24 h from ERA-Interim reanalysis data (http://apps.ecmwf.int/datasets/data/interim-full-daily/levtype=sfc/). PAR was calculated by multiplying the shortwave incident radiation (SW_{in}) by the ratio of SW_{in} to PAR (Ryu et al., 2018) in different PFTs for each 8 days interval. Finally, PAR was averaged over each 8-day interval and expressed as MJ m^{-2} at the site scale.

We used the Global LAnd Surface Satellite (GLASS) leaf area index (LAI) product (Xiao, Liang, Sun, Wang, & Jiang, 2015) to evaluate the LAI intra-annual variance at different PFTs. All the data here were aggregated into 8-day means to conform to the MOD17A2 GPP product

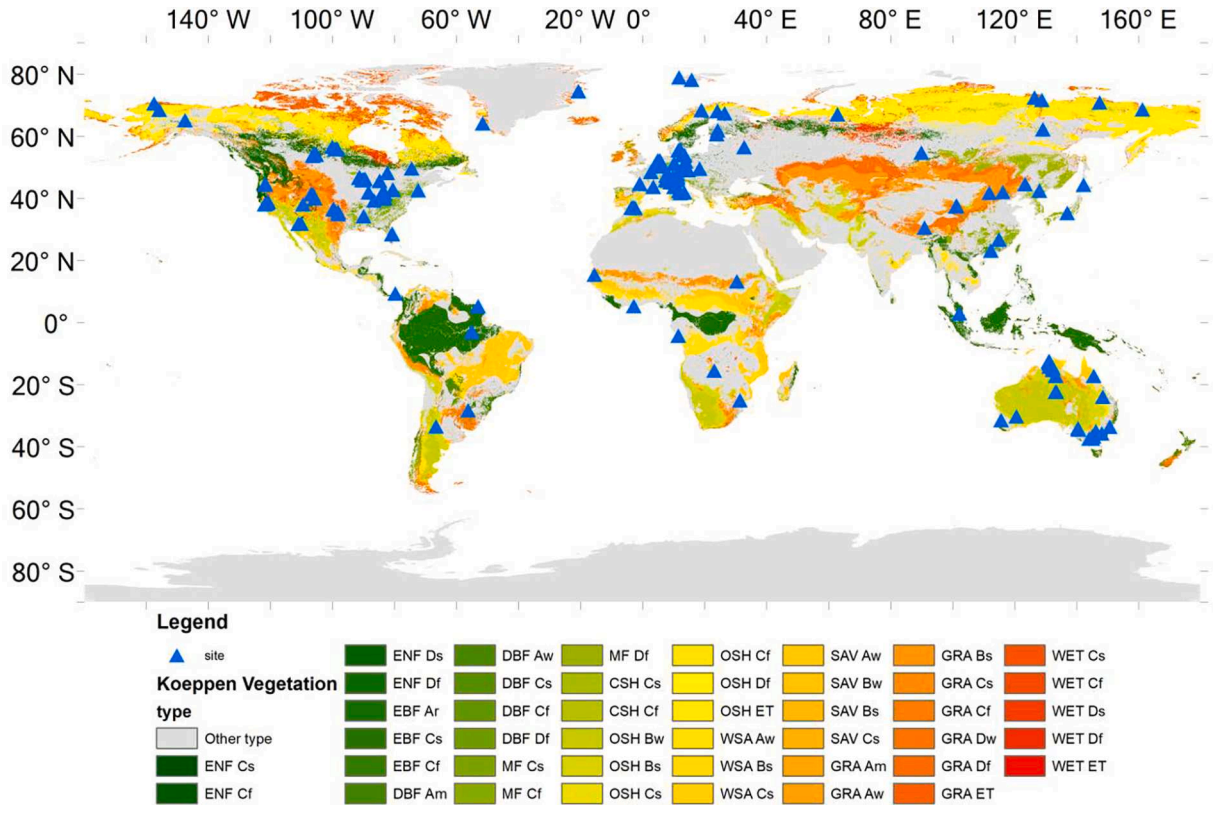

Fig. 1. Natural Plant Functional Types (PFTs) was overlapped by International Geosphere Biosphere Programme (IGBP) land cover classification and Köppen climate type. The first two or three letter of the plant functional type is the abbreviation of vegetation type (DBF- deciduous broadleaf forest, EBF-evergreen broadleaf forest (EBF), ENF-evergreen needleleaf forest (ENF), MF-mixed forest (MF), SAV-savanna (SAV), WSA-woody savanna (WSA), OSH- open shrub (OSH), CSH-close shrub (CSH), GRA-grass (GRA), WET-wetland (WET). The abbreviation after each vegetation type is climate type: Ar-rainforest (Ar), Am- tropical monsoon (Am), Aw-tropical woody savanna area (Aw), BW-arid desert (BW), BS-arid steppe (BS), Cf-temperate humidity/monsoon (Cf), Cs-Mediterranean (Cs), Cw-temperate dry (Cw), Df-boreal humidity (Df), Ds-boreal dry summer (Ds), Dw- boreal dry winter (Dw), ET- polar tundra. Other types, including cropland, urban area, deciduous needleleaf forest, non-vegetation cover, were excluded from this study.

Table 1
List of selected sites used in this study. Site years represent the number of carbon flux data years used in this study. The climate type is from the Köppen climatic classification. Vegetation type is deciduous broadleaf forest (DBF), evergreen broadleaf forest (EBF), evergreen needleleaf forest (ENF), mixed forest (MF), savanna (SAV), woody savanna (WSA), open shrub (OSH), close shrub (CSH), grass (GRA), wetland (WET). Climate type is rainforest (Ar), monsoon (Am) and woody savanna area (Aw), arid desert (BW) arid steppe (BS), temperate humidity/monsoon (Cf), Mediterranean (Cs), temperate dry (Cw), boreal humidity (Df), boreal dry summer (Ds), boreal dry winter (Dw), polar tundra (ET). All the selected sites and locations are listed in supplementary (Table S1).

Vegetation type	Climate type	PFT name	Sites	Site years
CSH	Cf	temperate monsoon close shrub	1	4
	Cs	Mediterranean close shrub	1	11
DBF	Am	tropical monsoon deciduous broadleaf forest	1	3
	Aw	woody savanna deciduous broadleaf forest	1	9
	Cf	temperate monsoon deciduous broadleaf forest	4	29
	Cs	Mediterranean deciduous broadleaf forest	4	27
	Df	boreal humidity deciduous broadleaf forest	13	115
EBF	Ar	tropical rainforest	4	32
	Cf	temperate monsoon rainforest	6	33
	Cs	Mediterranean evergreen broadleaf forest	3	26
ENF	Cf	temperate monsoon evergreen needleleaf forest	6	53
	Cs	Mediterranean evergreen needleleaf forest	2	9
	Df	boreal humidity evergreen needleleaf forest	29	248
	Ds	boreal dry summer evergreen needleleaf forest	3	24
GRA	Am	tropical monsoon grassland	1	3
	Aw	woody savanna grassland	2	14
	BS	arid grassland	3	21
	Cf	temperate monsoon grassland	12	57
	Cs	Mediterranean grassland	1	14
	Df	boreal humidity grassland	9	77
	Dw	boreal dry winter grassland	4	12
	ET	polar grassland	3	32
MF	Cf	temperate monsoon mixed forest	3	33
	Df	boreal humidity mixed forest	4	51
	Dw	boreal dry winter mixed forest	1	3
OSH	Bs	arid steppe open shrub	3	18
	Bw	arid desert open shrub	1	6
	Cs	Mediterranean open shrub	1	10
	Df	boreal humidity open shrub	3	15
	ET	polar open shrub	1	12
SAV	Aw	tropical savanna	3	18
	BS	arid steppe savanna	2	18
	BW	arid woody savanna	2	9
	Cs	Mediterranean savanna	1	4
WET	Cf	temperate monsoon wetland	3	13
	Cs	Mediterranean wetland	2	5
	Df	boreal humidity wetland	8	43
	Dw	boreal dry winter wetland	1	3
	ET	polar wetland	4	21
WSA	Aw	tropical woody savanna	3	20
	BS	arid steppe woody savanna	1	11
	Cs	Mediterranean woody savanna	1	14

time steps.

2.3. Description of GPP_{PFT} model

We optimized the GPP estimation model named GPP_{PFT} with the concept of maximal GPP (Richardson et al., 2007) by considering the difference of potential maximal GPP ($GPP_{POT,PFT}$) and vegetation growth stress in various plant functional types:

$$GPP = GPP_{POT,PFT}(LAI, PAR) \times F_{dominant,PFT}[f_{PFT}(T), g_{PFT}(VPD)] \quad (1)$$

Under various levels of PAR and phenological conditions, the potential maximal GPP in each PFT was presented as $GPP_{POT,PFT}(LAI,PAR)$. The LAI changed with canopy structure and phenological conditions, affecting the $GPP_{POT,PFT}$. The function is presented as:

$$GPP_{POT,PFT}(LAI, PAR) = LAI \times k_{p1,PFT} \times PAR^{k_{p2,PFT}} \quad (2)$$

The term $k_{p1,PFT} \times PAR^{k_{p2,PFT}}$ is a simplification of the light response function (Ide et al., 2010).

Because of the interrelationship of temperature, VPD, and PAR, here we follow the assumption that vegetation growth is mostly stressed by the dominant climate control factor of either temperature or VPD. In this research, climate stress is defined as the ratio between GPP and $GPP_{POT,PFT}$. The climate stress to $GPP_{POT,PFT}$ was considered to be the dominant climatic stress function ($F_{dominant,PFT}$) in equation (1) between 8-day mean temperature stress or 8-day mean VPD stress at each PFT, which were represented by $f_{PFT}(T)$and $g_{PFT}(VPD)$, respectively. When the dominant climate control factor is temperature, the $F_{dominant,PFT}$ equals to $f_{PFT}(T)$. Otherwise, the $F_{dominant,PFT}$ equals to $g_{PFT}(VPD)$ when the control factor is water. The dominant climate impact factor is defined as the factor with the highest R^2.

For the PFTs that had temperature as the dominant climate impact factor, the scalars were calculated according to (Sendall et al., 2015):

$$f_{PFT}(T) = A_{opt,PFT} - k_{T,PFT} \times (T - T_{opt,PFT})^2 \quad (3)$$

where the $A_{opt,PFT}$ is the temperature stress to photosynthesis under the optimal growing temperature ($T_{opt,PFT}$), and $k_{T,PFT}$ is the coefficient describing the scaled stress. The stress function of PFT controlled by water is (Jarvis, 1976):

$$g_{PFT}(VPD) = B_{opt,PFT} \times \exp(k_{w,PFT} \times VPD) \quad (4)$$

where the $B_{opt,PFT}$ is the water stress when VPD equals 0, and $k_{w,PFT}$ is strength of the water constraint.

2.4. Parameterization

To derive the model coefficients in GPP_{PFT} and select the dominant factor in each PFT, in each iteration, we randomly chose 70% of data in each PFT as the calibration set and the remaining 30% as the validation set. Firstly, we used the data in the calibration set to compute the model coefficients. The $GPP_{POT,PFT}(LAI, PAR)$ of equation (2) was fitted by a three-dimensional surface in each PFT where maximal LAI in this PFT was higher than 1.5 m^2 m^{-2}. We separated the PAR into 20 levels and LAI into 5 levels in each PFT, and then we selected the GPP values higher than the 95th percentiles under each LAI and PAR level as the $GPP_{POT,PFT}(LAI, PAR)$, to derive the coefficient k_{p1}, k_{p2} with that level of LAI and PAR and the least square adjustment method. The maximal GPP (GPP_{max}) of each PFT were derived from the $GPP_{POT,PFT}(LAI, PAR)$ with maximal LAI and maximal PAR. At the PFT whose maximal LAI was less than 1.5 m^2 m^{-2}, $GPP_{POT,PFT}$ was modelled by:

$$GPP_{POT,PFT}(PAR) = k_{pa1,PFT} \times PAR^{k_{pa2,PFT}} \quad (5)$$

where $GPP_{POT,PFT}(PAR)$ is the maximal GPP under different levels of PAR.

Secondly, we derived the coefficients in the dominant stress function ($F_{dominant,PFT}[(T), g_{PFT}(VPD)]$). For each calibration set of each PFT, we calculated the $GPP_{POT,PFT}$ with LAI and PAR input and the coefficient calculated in the first step. Then, we derived the term $F_{dominant,PFT}[(T), g_{PFT}(VPD)]$ as the ratio of each GPP_{flux} to $GPP_{POT,PFT}$. Next, we used the ratio of GPP_{flux} to $GPP_{POT,PFT}$ with 8-day mean temperature and 8-day mean VPD, to derive the model coefficients with equation (3) and (4) by the least square adjustment method. The dominant control factor

between T and VPD was selected as the one that had a fitting R^2 higher than 0.2 and an RMSE lower than the other factor's function. If both the fitting R^2 were lower than 0.2, the dominant factor was selected as the factor with higher intra-annual variance in coefficient of variation (CV) of T or VPD.

Thirdly, we derived all the coefficients in $GPP_{POT,PFT}$, $f_{PFT}(T)$, $g_{PFT}(VPD)$ and the dominant factor in each PFT. Then, we repeated this iteration 10,000 times. Next, we summarized the coefficients of $GPP_{POT,PFT}$, $f_{PFT}(T)$, $g_{PFT}(VPD)$ and the dominant factor in each PFT during the 10,000 iterations into the PFT trait look up table (Fig. 2).

Next, we used all the 8-day mean temperature, VPD, PAR and 8-day LAI data for the selected site with the PFT trait look up table to derive GPP_{PFT} in all the PFTs and then summarize them into each vegetation type. Lastly, we cross-compared our results with satellite-based 1 km spatial resolution GPP products including the Breathing Earth System Simulator (GPP_{BESS}, (Jiang and Ryu, 2016)), the Vegetation Photosynthesis Model (GPP_{VPM}, (Zhang et al., 2017)), and MODIS-GPP (GPP_{MOD}, (Running et al., 2004)) from 2001 to 2014. We summarized GPP_{PFT}, GPP_{MOD}, GPP_{VPM} and GPP_{BESS} into 1-km^2 results near the center of the flux towers, then compared them to GPP_{FLUX} for the same time from 2001 to 2014 as the cross-validation results.

3. Results

3.1. Maximum GPP across PFT

Table 2 shows the maximal GPP differs in different PFTs. Within the same vegetation type, the GPP_{max} has a high difference with at least 3 g C m^{-2} day^{-1} across different climate zones. For example, while the GPP_{max} in deciduous broadleaf forest in tropical (DBF_Am) is around 8 g C m^{-2} day^{-1}, in the temperate zone (DBF_Cf) it is higher than 19 g C m^{-2} day^{-1}. Similarly, the GPP_{max} also has a high variance across different climatic zones in grassland (GRA), and in the polar grassland (GRA_ET) the GPP_{max} is around 4 g C m^{-2} day^{-1} while in the temperate monsoon region (GRA_Cf) it reaches 17 g C m^{-2} day^{-1}. Open shrub (OSH) also has high variance; its GPP_{max} in the boreal zone (OSH_Df) is around 8 g C m^{-2} day^{-1}, which is three times higher than in the arid zone (OSH_BW). Generally, the GPP_{max} is higher in temperate and boreal monsoon zones.

Fig. 3 shows modeled results for the potential maximal daily GPP (GPP_{POT}) in different vegetation types across climate zones under a certain level of LAI. We compared GPP_{POT} across PFTs under clear sky day with PAR around 12 MJ. The GPP_{POT} shows strong differences across PFTs. In deciduous forests, the highest GPP_{POT} is found in the temperate monsoon zone, where daily GPP is around 25 g C m^{-2} day^{-1}. Under the same level of PAR, tropical woody savanna climate shows a similar GPP_{POT}. The GPP_{POT} is about 21, 14, 11 g C m^{-2} day^{-1} in the Mediterranean, boreal monsoon and tropical monsoon area, respectively. Evergreen broadleaf forest shows the least difference under high PAR, with GPP_{POT} of 16, 18, 14 g C m^{-2} day^{-1} in tropical rainforest, temperate monsoon, and Mediterranean area, respectively. In non-forest areas, GPP_{POT} is lower since the LAI is also lower than in the forest areas. The highest GPP_{POT} (~13 g C m^{-2} day^{-1}) in grassland is found in the tropical woody savanna area. The second highest GPP_{POT} is found in the temperate monsoon area (~11 g C m^{-2} day^{-1}), which is around 3, 1, 10 g C m^{-2} day^{-1} higher than in the tropical monsoon, boreal monsoon, and polar area, respectively. Low GPP_{POT} in grassland was found for GRA_ET and GRA_Dw with high mean shortwave radiation to PAR ratios (>0.5). Savanna also has high GPP variance under high PAR. The highest GPP_{POT} is found in the arid area around 11 g C m^{-2} day^{-1} and it is 2 and 6 g C m^{-2} day^{-1} higher than in tropical and temperate areas. At same PFTs such as DBF_Am and GRA_Am showed only small GPP_{POT} variance under different levels of PAR.

3.2. Physiological stress to $GPP_{POT,PFT}$

Table 2 shows the transfer ratio of shortwave radiation to PAR in different PFTs. Generally, the ratio is lower in tropical PFTs, mostly around 0.44 to 0.48. The ratio is higher in temperate PFTs, where it is around 0.47 to 0.49. The higher ratios are found in highland PFT (WET_Dw, 0.514) and in the polar PFT (GRA_ET, 0.509). Fig. 4c shows that PAR in dry regions (e.g. GRA_BS, WSA_Aw) changes little throughout the year, with less than 5 MJ difference between days.

Fig. 4a shows that for the same vegetation type in the tropical and dryland zones (A and B in the Köppen classification), the daily mean temperature is 10 to 15 °C higher than in temperate zones, and in temperate zones it is approximately 10 °C higher than in boreal regions (type D). Meanwhile, the intra-annual temperature variance in tropical and dryland PFTs is less than 10 °C. However, temperature shows a higher variance of >30 °C in temperate and boreal regions than others. Fig. 4b shows that VPD has a higher variance in tropical and dryland

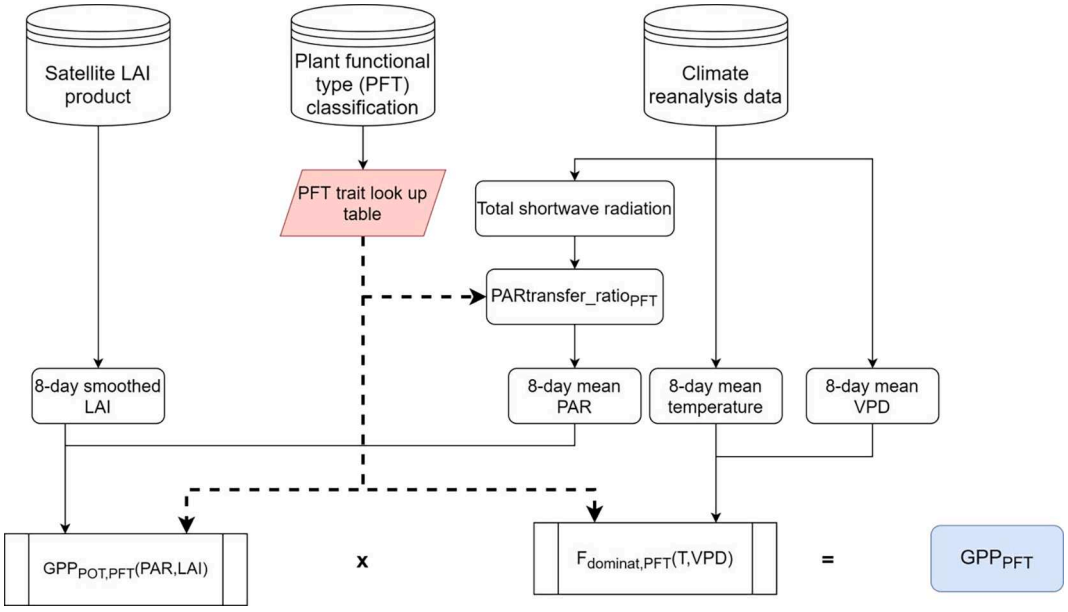

Fig. 2. Flow chart of the estimation of GPP by considering difference of plant functional type information. Solid lines represent the data flow while dashed lines indicate the plant trait and climate stress function of different plant functional types.

Table 2
Daily maximal GPP, maximal LAI derived from the FLUXNET2015, and vegetation growth dominant factor in different Plant Functional Types (PFTs).

PFTs	Mean ratio from shortwave radiation to PAR	Daily maximal GPP (gC m^{-2} day^{-1})	LAI max (m^2 m^{-2})	Temperature dominant (%)	VPD dominant (%)
CSH_Cf	0.469	8.80	3.56	1.6	98.4
CSH_Cs	0.479	5.76	2.00	100.0	0.0
DBF_Am	0.442	7.66	3.95	1.9	98.1
DBF_Aw	0.484	7.88	3.56	0.9	99.1
DBF_Cf	0.479	19.57	4.88	100.0	0.0
DBF_Cs	0.480	16.62	4.68	100.0	0.0
DBF_Df	0.478	17.43	6.02	100.0	0.0
EBF_Ar	0.441	15.40	5.70	0.9	99.1
EBF_Cf	0.476	14.87	4.81	98.0	2.0
EBF_Cs	0.481	12.19	4.76	2.1	97.9
ENF_Cf	0.474	13.92	4.20	100.0	0.0
ENF_Cs	0.490	7.62	4.19	100.0	0.0
ENF_Df	0.483	15.60	4.50	100.0	0.0
ENF_Ds	0.491	11.22	3.41	100.0	0.0
GRA_Am	0.442	13.32	4.71	0.0	100.0
GRA_Aw	0.467	13.64	3.41	0.0	100.0
GRA_BS	0.482	10.47	1.49	99.2	0.8
GRA_Cf	0.477	17.83	4.84	100.0	0.0
GRA_Cs	0.485	11.34	3.22	21.1	78.9
GRA_Df	0.482	17.89	4.50	100.0	0.0
GRA_Dw	0.506	12.89	2.00	100.0	0.0
GRA_ET	0.509	4.49	1.59	100.0	0.0
MIF_Cf	0.475	13.94	5.07	100.0	0.0
MIF_Df	0.479	14.39	5.35	100.0	0.0
MIF_Dw	0.496	13.82	5.37	100.0	0.0
OSH_BS	0.485	4.25	0.59	24.3	75.7
OSH_BW	0.474	1.95	0.86	100.0	0.0
OSH_Cs	0.477	3.06	0.80	100.0	0.0
OSH_Df	0.485	6.66	3.88	100.0	0.0
OSH_ET	0.489	6.53	2.07	100.0	0.0
SAV_Aw	0.458	10.91	2.00	66.4	33.6
SAV_BS	0.474	11.91	2.59	0.0	100.0
SAV_BW	0.480	14.14	1.63	6.1	93.9
SAV_Cs	0.478	6.56	2.18	34.2	65.8
WET_Cf	0.473	14.12	4.86	100.0	0.0
WET_Cs	0.480	16.53	2.46	95.7	4.3
WET_Df	0.478	11.92	4.90	100.0	0.0
WET_Dw	0.514	11.53	4.71	100.0	0.0
WET_ET	0.477	5.08	1.45	100.0	0.0
WSA_Aw	0.462	12.33	2.90	0.0	100.0
WSA_BS	0.483	6.22	0.61	0.0	100.0
WSA_Cs	0.485	9.52	2.52	0.0	100.0

zones (type A, B) than in temperate and boreal regions (type C, D), whereas temperature varies the least in the tropics (type A). Contrary to temperature, the intra-annual VPD variance is more significant in tropical and dryland zones, reaching about 30 hPa in some PFTs (e.g. DBF_Aw, GRA_BS). However, it changes less than 10 hPa in polar PFTs (e.g. WET_ET, GRA_ET). Most of the vegetation types we selected here span two or more climate zones. For instance, the OSH can be found in six climate zones, including arid steppe (BS), arid desert (BW), dry summer (Cs), boreal without dry summer (Df), boreal dry winter (Ds), polar tundra (ET), where the growing season mean temperature range from 3 to 22 °C. The GRA type is found in 5 major climate zones covering 8 PFTs, and the growing season mean temperature varies by 25 °C while the mean VPD has a 15 hPa difference among the climate zones. The average growing season temperature for EBF in the tropical zone is 25 °C, but it drops to 15 °C in the temperate zone.

The major climate control factor varies across different PFTs. Fig. 5 shows the correlation between temperature, VPD, LAI and PAR with GPP. Generally, daily temperature is very correlated with VPD in most PFTs, often with a Spearman's *r* higher than 0.7. However, the relationship between temperature and VPD is not significant in tropical and dry regions, with *r* less than 0.2 at DBF_Aw, GRA_Aw, SAV_Aw, SAV_BW. Temperature has a positive correlation with GPP in most of the temperate and boreal regions (type C and D) with r higher than 0.6. The VPD has a negative correlation with GPP in most dryland and tropical sites (e.g., DBF_Am, GRA_Cs, WSA_Aw) with r less than −0.4. However, there is no significant correlation between different climate factors and GPP at tropical rainforest sites (EBF_Ar). Table 2 also shows the dominant factor for vegetation growth at different PFTs after 10,000 iterations. Generally, 95% of vegetation growth in temperate, boreal and polar zones is controlled by temperature, while in tropical and dryland regions it is controlled more by VPD. For example, 100% of DBF growth in temperate monsoon (Cf), Mediterranean (Cs) and boreal monsoon region (Df) is controlled by temperature change. However, in tropical woody regions (Aw), DBF growth is majorly controlled by changes in VPD, while in tropical monsoon region (Am), 68% of DBF is controlled by changes in VPD and 32% is controlled by temperature.

Fig. 6 shows the dominant climatic stress function in some PFTs. In deciduous broadleaf forest (DBF), the optimal growth temperatures are 31, 27, 19 °C in the temperate humid (Cf), boreal humid (Df), Mediterranean (Cs) types, respectively, and under 10 hPa of VPD, the mean growth stress for the monsoon tropical rainforest (Am) is around 0.6 while for the dry tropical zone (Aw) it is 0.8. In EBF, the tropical rainforest has almost the same level of water stress (0.76) under a different level of VPD but Mediterranean forest has higher water stress (0.2) at 10 hPa. The climatic stress of grasslands (GRA) growth presents significant differences across climate zones. The optimal growth temperature is around 18, 13, 17, 27, 14 °C in dry desert (BS), temperate monsoon (Cf), boreal monsoon (Df), boreal dry (Dw), polar (ET) climate zone, respectively. When VPD is high (>15 hPa), the water stress for grasslands is more significant in tropical than in temperate regions. In the savannah (SAV), generally, under different levels of VPD, the Mediterranean savannah (Cs) has the least water stress (0.8), followed by the desert savannah (Bw, 0.7), while the savannah of the arid desert (BS) is the most stressed by VPD.

3.3. Intercomparison of GPP results

Fig. 7 shows the intercomparison of GPP from models and remote sensing products against flux tower-based GPP across all sites. The GPP_{PFT} model has the highest correlation ($R^2 = 0.77$) and the lowest RMSE (1.79 g C m^2 day^{-1}) with GPP_{flux}. The GPP_{BESS} product also has a high correlation ($R^2 = 0.73$) and low RMSE (1.95 g C m^2 day^{-1}) with GPP_{flux}. The products considering only vegetation type exhibit a higher uncertainty: GPP_{VPM} and GPP_{MOD} have a R^2 of 0.69 and 0.64 with GPP_{flux}, respectively, and an RMSE of 2.07 and 2.25 g C m^2 day^{-1}, respectively. All the models and products have a low daily mean bias with GPP_{flux} of less than 0.7 g C m^2 day^{-1}.

Table 3 shows the comparison of model and product GPP with GPP_{flux} in different vegetation types. Seven natural vegetation types, including CSH, DBF, EBF, GRA, MIF, WET, WSA, have high correlation ($R^2 > 0.7$) with GPP_{flux}. The highest correlation of GPP_{PFT} with GPP_{flux} is in DBF, with a R^2 of 0.85. However, sparse vegetation types SAV and OSH have lower correlations with GPP_{flux}, with R^2 of 0.59 and 0.61, respectively. The BESS product, which takes into account the Vcmax differs across PFT, has a high correlation with GPP_{flux}. Moreover, GPP_{PFT} has the lowest RMSE with GPP_{flux} in 7 vegetation types, while the rest three lowest RMSE values against GPP_{flux} were found in the GPP_{BESS} product. The products and models that consider plant trait differences across climate types (GPP_{PFT} and GPP_{BESS}) have higher correlation with GPP_{flux} in all natural vegetation types than the other two products that without incorporating plant trait differences, with at most 0.46 g C m^2 day^{-1} of RMSE reduction. The best improvement is measured for evergreen broadleaf forest. GPP_{PFT} has 0.31 of R^2 improvement and a reduction of at least 0.68 g C m^2 day^{-1} in RMSE than other products. Additionally, GPP_{PFT} of DBF also has a reduction of 0.34 g C m^2 day^{-1} in RMSE.

Fig. 8 shows the daily GPP variance in different climate zones for four vegetation types. Generally, GPP_{PFT} has a lower mean bias than

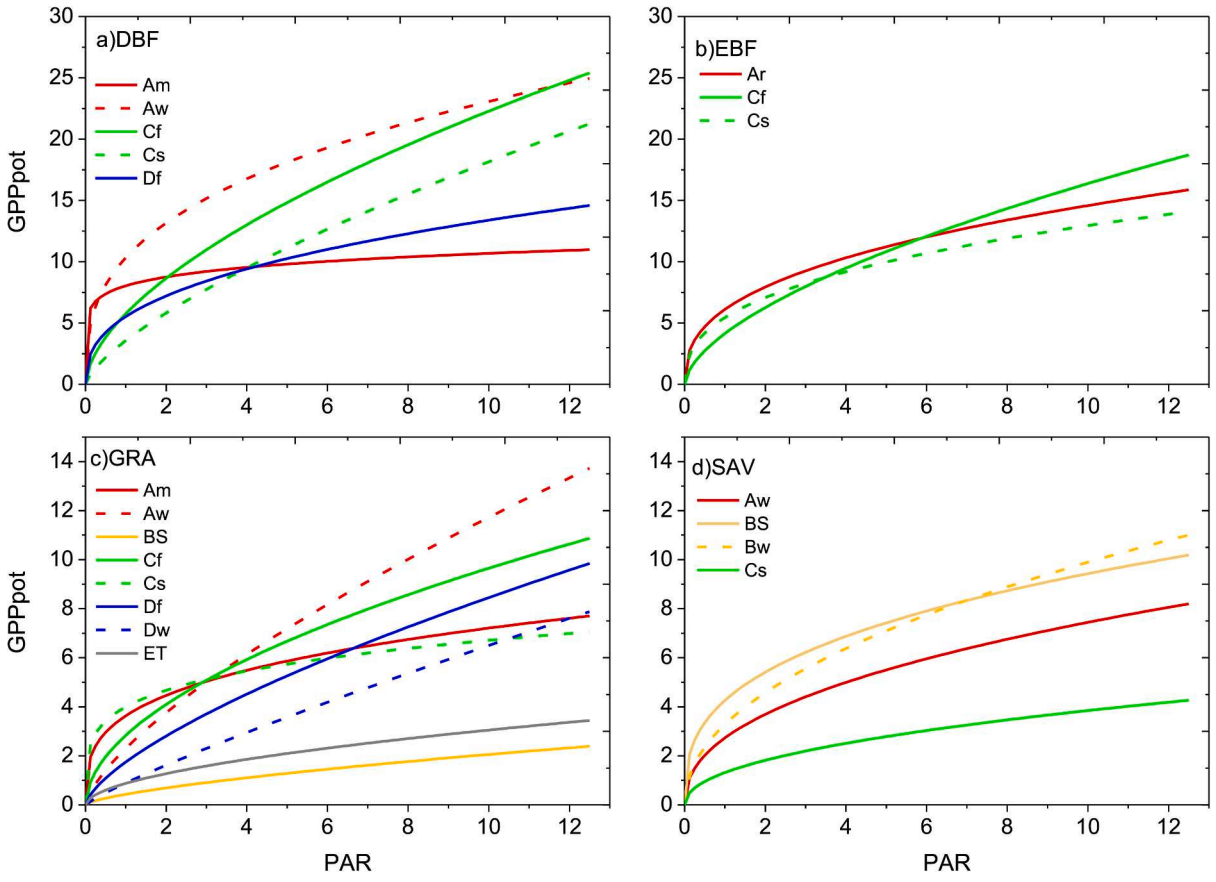

Fig. 3. Modeled potential maximal GPP (GPP_{POT}) in different PFTs. Here, GPP_{POT} in EBF and DBF sites are for LAI equal to 5 m^2 m^{-2}, while GPP_{POT} in GRA and SAV are for LAI equal to 2 m^2 m^{-2}. All the modeled GPP_{POT} with a $p < 0.05$. GPP_{POT} is in g C day^{-1} and PAR is in MJ day^{-1}.

GPP_{MOD}. Daily mean GPP derived from GPP_{PFT} of all the PFTs of GRA, SAV, EBF and DBF sites are almost on the 1:1 line and most of the estimates have less than 1 g C m^2 day^{-1} bias with GPP_{flux}. Besides, the mean GPP of each vegetation type has high variance in different climate zones. For example, the mean GPP in the grassland of the tropical areas is 8 g C m^2 day^{-1}, but it is 1.2 g C m^2 day^{-1} in the polar areas (Fig. 8a1). The mean GPP in evergreen broadleaf forest in tropical areas is 9.3 g C m^2 day^{-1}, but is 4.5 g C m^2 day^{-1} in the Mediterranean areas (Fig. 8c1). However, the GPP results for some PFT have a high bias with GPP_{flux}. Unlike GPP_{PFT}, GPP_{MOD}, which did not consider climate zone plant trait differences, has >3 g C m^2 day^{-1} bias with GPP_{flux} in GRA_Am (Fig. 8c2). Similarly, GPP_{MOD} has a significant mean GPP bias with GPP_{flux} in SAV_Cs, SAV_BS and SAV_BW, with >1 g C m^2 day^{-1} bias with GPP_{flux} (Fig. 8b2). In forest sites, GPP_{MOD} of EBF in the Mediterranean climate zone (Cs) also has 2.08 g C m^2 day^{-1} bias with GPP_{flux}. GPP_{MOD} of DBF in the Mediterranean climate zone (Cs), woody savannah (Aw), temperate humidity (Cf) has 1 g C m^2 day^{-1} bias with GPP_{flux} (Fig. 8d2).

4. Discussions

4.1. $GPP_{POT,\ PFT}$ reflects the GPP_{max} in PFTs

Plant traits for photosynthesis are very different across PFTs (Bonan et al., 2015), and $GPP_{POT,\ PFT}$ modelled the plant trait of GPP_{max} across the PFT. Our results showed that GPP_{max} not only has high variance across vegetation types but also varies strongly across climate zones even within the same vegetation type; thus, it is highly different across PFTs. Compared to the traditional GPP model that uses a constant canopy scale LUE_{max} (Running et al., 2004) or constant GPP_{max} (Richardson et al., 2007), our study used $GPP_{POT,\ PFT}$ to model the GPP_{max} across the PFT, which indicated the photosynthetic plant trait differences (Fig. 3). For example, daily GPP_{max} had a large difference (Table 2) between the tropical and the temperate zone of deciduous forests. High latitude areas in the summertime have long daylight, which potentially leads to high daily incident PAR and is conducive to high GPP_{max}. Table 2 shows that vegetation in temperate and boreal zones have higher GPP_{max} than the tropical zone, which is consistent with previous research (Zhang et al., 2016, 2017). The modelled $GPP_{POT,PFT}$ also have higher variance across PFTs (Fig. 3). More significant differences were found in forest sites, because these have a higher vegetation component that leads to higher daily average GPP (Zhang et al., 2016). A similar pattern exists in leaf scale maximum carboxylation rate (Vcmax), which differs largely across climate zones and species (Groenendijk et al., 2011). Thus, $GPP_{POT,\ PFT}$ linked the difference of plant trait for photosynthesis across PFTs.

The $GPP_{POT,\ PFT}$ modelled the GPP_{max} well under different levels of incident PAR across PFTs. First, the PAR from $GPP_{POT,\ PFT}$ incorporates diffuse and direct fractions from SW to PAR from different PFTs. Since the transfer ratio from SW to PAR varies across PFTs (Ryu et al., 2018), the polar zone has a higher direct component of radiance, which results in the polar vegetation type having lower GPP_{max} (Table 2) than other PFT with same SW. Canopy stress caused by large amounts of direct PAR causes GPP to decrease. Thus, accounting for the diffuse ratio in different PFTs and PAR variance allows to successfully quantify the amount of $GPP_{POT,\ PFT}$. Second, $GPP_{POT,\ PFT}$ considered the light response function of GPP_{max} (Eq. (2)) and this modelled the saturation point of GPP_{max} in different PFTs. The traditional LUE models omitted the influence of PAR on LUE_{max} (Zhang et al., 2018). Fig. 3 showed that GPP_{POT} is almost saturated at 8 g C m^2 day^{-1} with 4 MJ day^{-1} in tropical monsoon DBF, but keeps increasing for other PFTs in DBF. This is because when daily incident PAR is low, the canopy is assumed to receive more diffuse light, leading to higher LUE, which corresponds to a

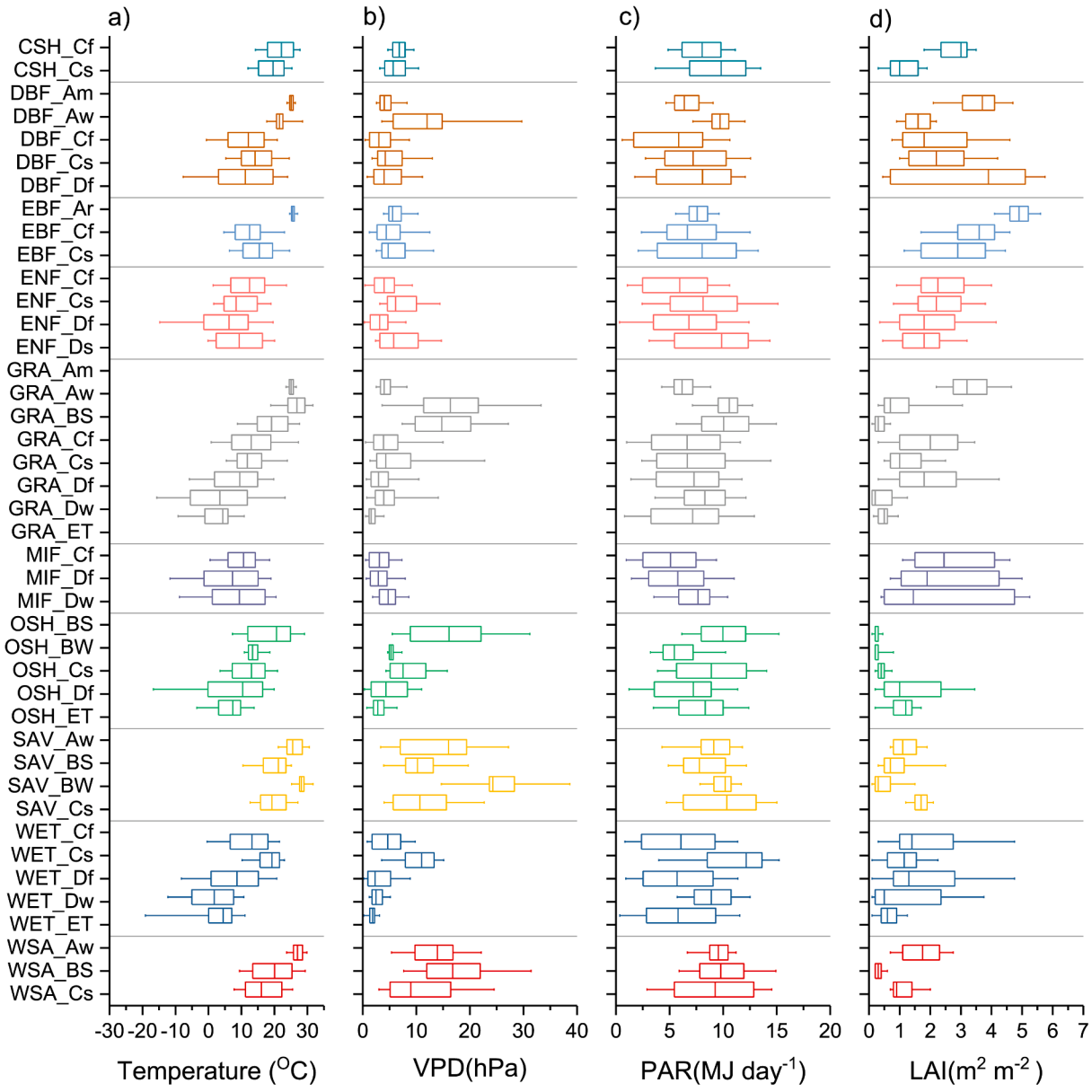

Fig. 4. Boxplots showing inter-annual variability in temperature, VPD, PAR and LAI in various PFTs of selected sites during the growing season (GPP > 5% of the maximum GPP in that PFT). The whisker on the left represents the first percentile, while the right whisker is the 99th percentile. The left and right boundaries of the box correspond to the 25th and 75th percentiles, respectively. The mean value is marked as the vertical line in the box corresponds to the average value in this PFT.

rapid increase in GPP (He et al., 2018); when the canopy receives higher daily incident PAR, it has lower LUE because it has higher direct light stress, and $GPP_{POT,\ PFT}$ will increase less after the PAR saturation point (Ide et al., 2010). Third, $GPP_{POT,\ PFT}$ modelled the PAR control differently in different PFTs (Fig. 4). Fig. 4 shows that GPP has a low correlation with PAR in DBF_Am. Because the GPP_{max} of DBF_Am are mostly near the saturation point of GPP, GPP is mostly stressed by water (Kumagai et al., 2015). However, other PFTs in DBF (e.g., DBF_Cf), are significantly correlated to PAR and temperature (Verbeeck et al., 2008).

$GPP_{POT,PFT}$ modelled maximal GPP under different phenological conditions (Fig. S1). At different stages of vegetation growth, phenology conditions change the canopy structure, especially the LAI and pigment pools, resulting in different photosynthetic capacity (Lin et al., 2017). Maximal GPP_{POT} appears in the peak of the growing season. At this time, the canopy has the highest pigment pools and maximal LAI. This is in agreement with the conclusion that ecosystems with higher LAI have the potential to produce more GPP (Rogers et al., 2017). Minimal GPP_{POT} appears when the canopy has least LAI. At this time, GPP is much less than in the summer because it is in the green-up stage. With this improvement, $GPP_{POT,PFT}$ can identify GPP_{max} of different vegetation periods, reducing early spring overestimation of GPP and underestimation of GPP_{max} during the peak of summer.

4.2. Climate stress variance in PFTs

The dominant climate control factor is different across PFTs (Figs. 5 and 6, Table 2) and $F_{dominant,PFT}$ quantifies it well. $F_{dominant,PFT}$ showed that vegetation growing in temperate, boreal and polar climates is controlled by temperature changes (Table 2), which is in agreement with previous results (Nemani et al., 2003; Piao et al., 2011; Madani et al., 2017). Temperature changes significantly in these climate zones, with intra-annual variance mostly higher than 25 °C (Fig. 4). GPP is strongly correlated with temperature within the year (Fig. 5). When temperature tends to be below zero, and extreme low temperatures significantly limit plants' photosynthesis, the dominant climatic stress function shows correctly a low value. When air temperature reaches the

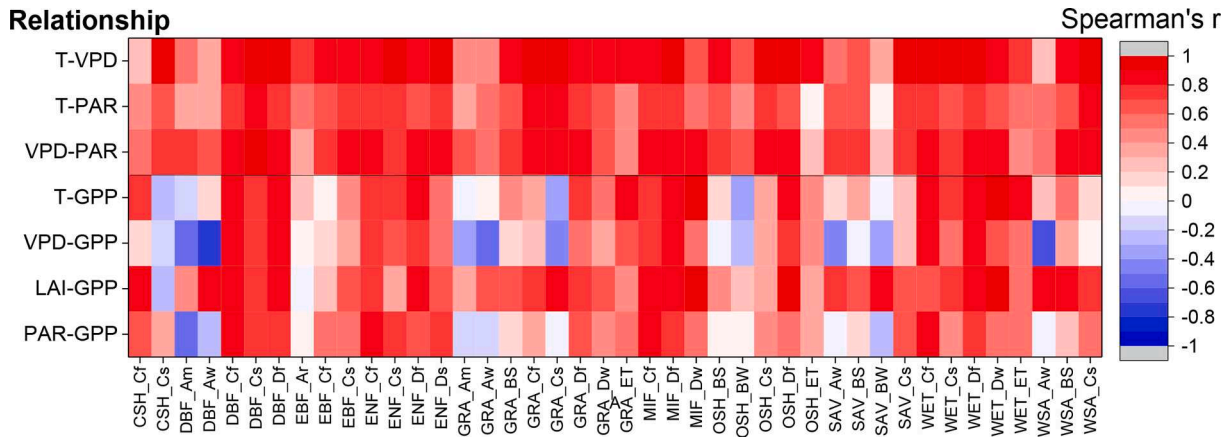

Fig. 5. Correlations between different input variables including temperature (T), VPD, PAR, LAI, and between input variables and GPP, across the different PFTs. Data were aggregated to 8-day intervals.

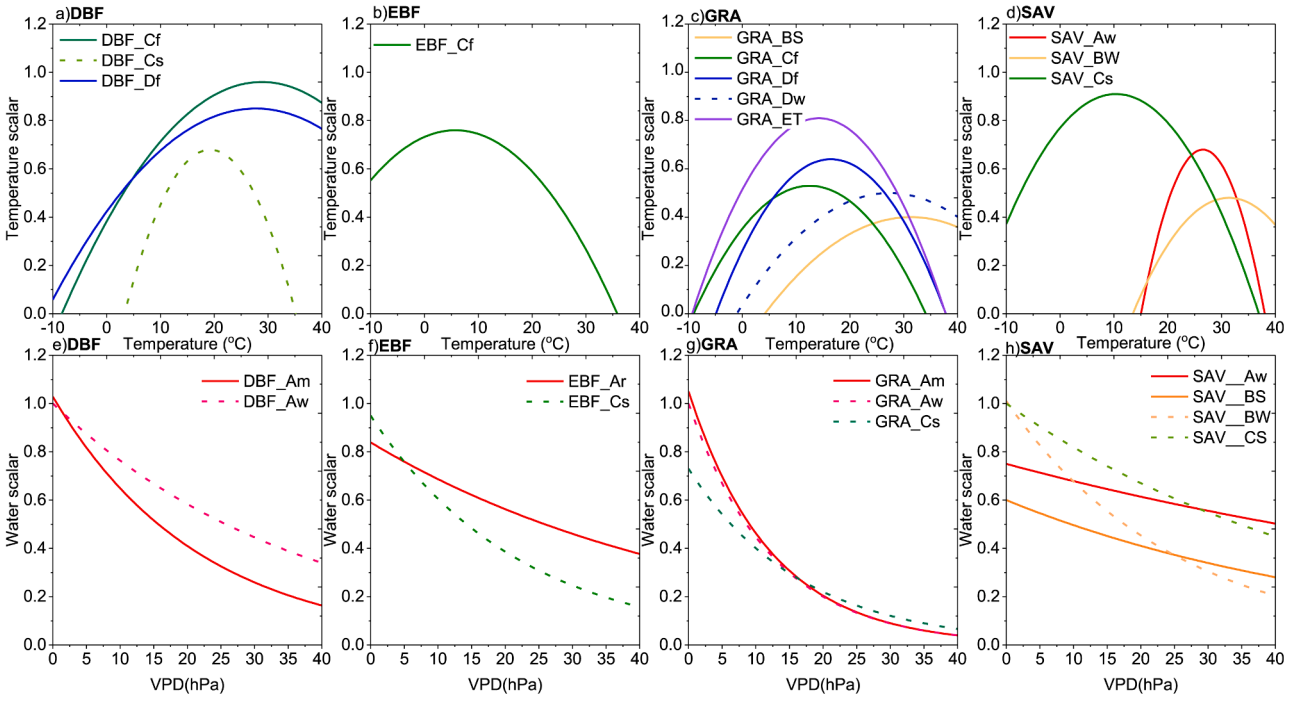

Fig. 6. PFT growing response to environmental factors for the GPP_{PFT} method. Panels a-d report the temperature stress function in the select PFTs, fitted by equation (2). Panels e-h report the water stress function fitted by equation (3). Each subfigure shows the growth response function of the dominant factor at that PFT. The growth response functions are shown for four vegetation types, including DBF (deciduous broadleaf forests), EBF (evergreen broadleaf forest), GRA (grass), and SAV (savanna), which span more than three climate zones. The coefficients of the fitted curve are reported in supplementary Table S4.

optimal growth temperature, the canopy reaches the highest GPP (Sendall et al., 2015). When air temperature is higher than the optimal growing temperature, photosynthetic capacity starts to decline as the transfer rate of CO_2 limits photosynthesis under high temperatures (Bernacchi et al., 2002). Thus, the fact that temperature well correlated to the GPP indicates that the climate control factor is temperature for these PFTs (Dass et al., 2015).

The result from $F_{dominant,PFT}$ (Table 2) fits the conclusion that the dominant climate control factor for vegetation growth in tropical and arid areas is VPD (Madani et al., 2017; Grossiord et al., 2020). Unlike the PFT controlled by temperature, these PFTs have low intra-annual temperature variance, mostly lower than 15 °C, but have intra-annual VPD variance. Thus, in regions such as the Mediterranean close shrub (CSH_Cs), Mediterranean grassland (GRA_Cs), arid woody open shrub (OSH_BW), the relationship between temperature and GPP is negative ($r < -0.2$) since here there is a modest intra-annual variance in temperature. In these PFTs, the minimum temperature is usually higher than 0 and rainfall significantly affects the intra-annual variance of VPD Grossiord, Sevanto, Limousin, et al., 2017. When the temperature does not pose a high stress to vegetation growth, a drought effect on photosynthesis appears, and the relationship between VPD and GPP becomes robust (Grossiord, et al., 2020).

The dominant climatic stress function also showed that similar climatic conditions lead to different stress to vegetation growth across PFTs. Although the dominant control factor is the same, Fig. 6 shows that temperature scalars are different at the same temperature across PFT. This is because plant traits such as the optimal growth temperature are very different across PFT (Sendall et al., 2015; Slot and Winter, 2017). Thus, temperature stress to the vegetation growth is different across PFTs. Our results are consistent with previous studies that showed

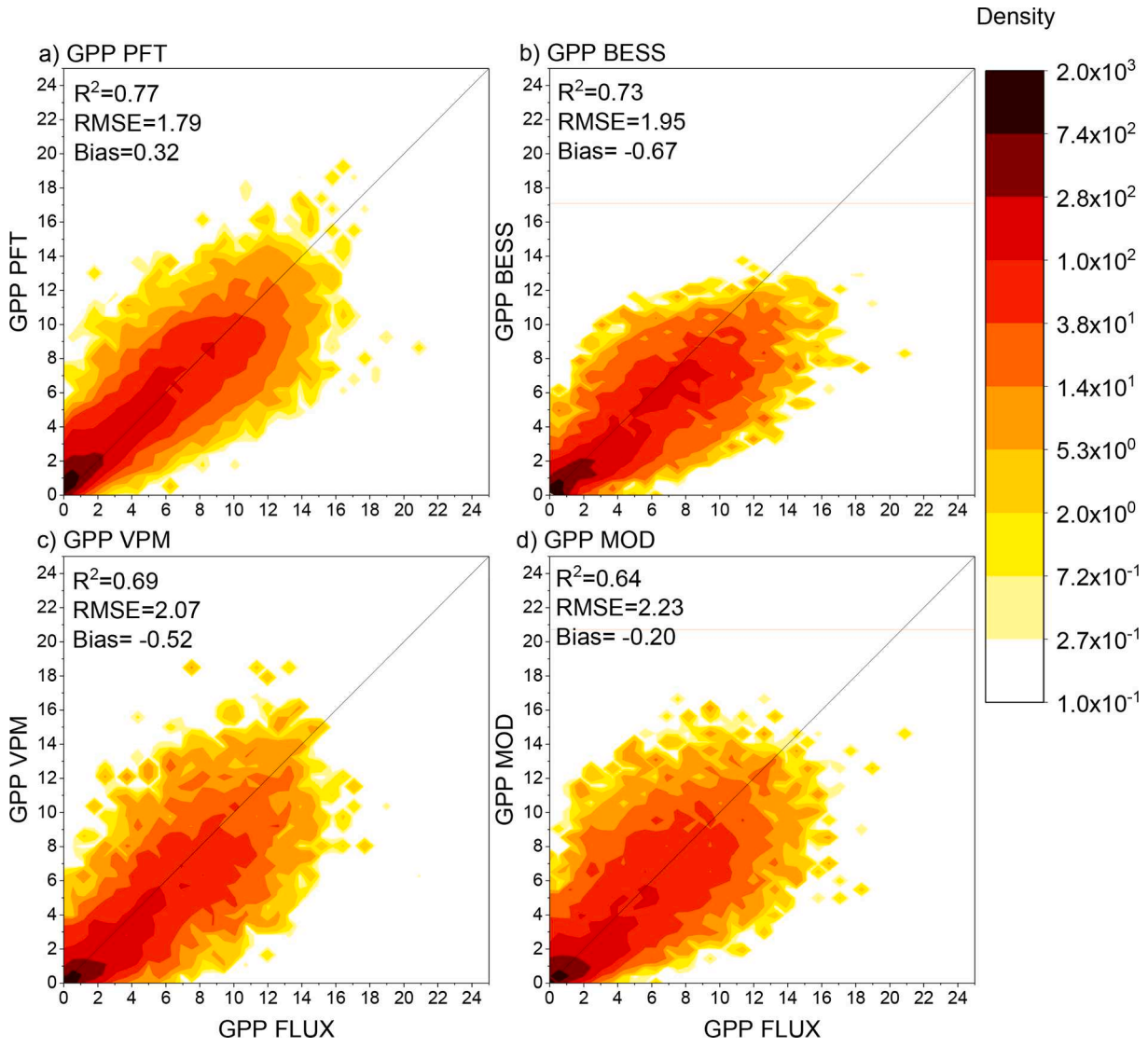

Fig. 7. Comparison between carbon flux tower-based GPP (GPP FLUX) and different model and remote sensing products-based GPP at 8-day composites GPP, RMSE, and Bias are in g C m^2 day^{-1}. The solid diagonal line represents the 1:1 line.

Table 3
Comparison of modeled GPP with separate climate zones (PFT) and the MODIS GPP product (MOD), the VPM GPP product (VPM), and the BESS GPP product (BESS) against flux tower based GPP. The numbers in bold font indicate higher R^2, lower RMSE, lower absolute bias than the other models. RMSE and bias are given in g C m^{-2} day^{-1}. The GPP estimation relationship between modeled GPP with GPP_{flux} in each PFT is in supplementary Table S3.

	PFT R^2	MOD R^2	VPM R^2	BESS R^2	PFT RMSE	MOD RMSE	VPM RMSE	BESS RMSE	PFT Bias	MOD Bias	VPM Bias	BESS Bias
CSH	**0.73**	0.27	0.60	0.70	**0.85**	1.40	1.04	0.89	**0.04**	1.49	−0.21	0.96
DBF	**0.85**	0.77	0.76	0.79	**1.79**	2.22	2.31	2.13	0.47	**0.22**	−0.23	−0.54
EBF	**0.66**	0.35	0.34	0.35	**1.77**	2.46	2.46	2.45	**−0.02**	0.74	−1.86	−1.40
ENF	0.74	0.69	0.71	**0.76**	1.70	1.88	1.82	**1.66**	0.67	**−0.61**	−0.87	−0.98
GRA	0.70	0.61	0.68	**0.72**	2.02	2.33	2.09	**1.98**	**−0.14**	−0.93	−0.31	−0.50
MIF	**0.79**	0.76	0.77	**0.79**	**1.62**	1.74	1.70	1.63	0.37	−0.25	**0.06**	−0.34
OSH	0.61	0.46	0.50	**0.67**	0.91	1.07	1.02	**0.83**	0.26	0.32	**−0.03**	0.19
SAV	**0.59**	0.35	0.57	0.44	**1.62**	2.02	1.65	1.89	**−0.18**	1.08	0.52	−0.81
WET	**0.74**	0.68	0.69	0.72	**1.77**	1.97	1.92	1.84	0.87	−0.76	−0.15	**−0.01**
WSA	**0.76**	0.62	0.75	0.53	**1.33**	1.66	1.35	1.86	**−0.36**	1.32	−0.37	−0.82

that temperature stress is different under the same temperature in some temperate and boreal tree species (Sendall et al., 2015). We also found that VPD scalars are different across PFTs under the same VPD (Fig. 6), because photosynthesis in PFTs has different sensitivity to VPD (Grossiord et al., 2020). For instance, the arid savanna is stressed more by insufficient water availability than tropical and Mediterranean savanna (Fig. 6). This finding is in agreement with previous research that showed that arid vegetation is controlled more by water limitations (Sjöström et al., 2013; Kanniah et al., 2013). Our results also show that tropical grassland shows higher sensitivity to water stress than the Mediterranean one, which is consistent with previous results (Sjöström et al., 2013; Wagle, 2015).

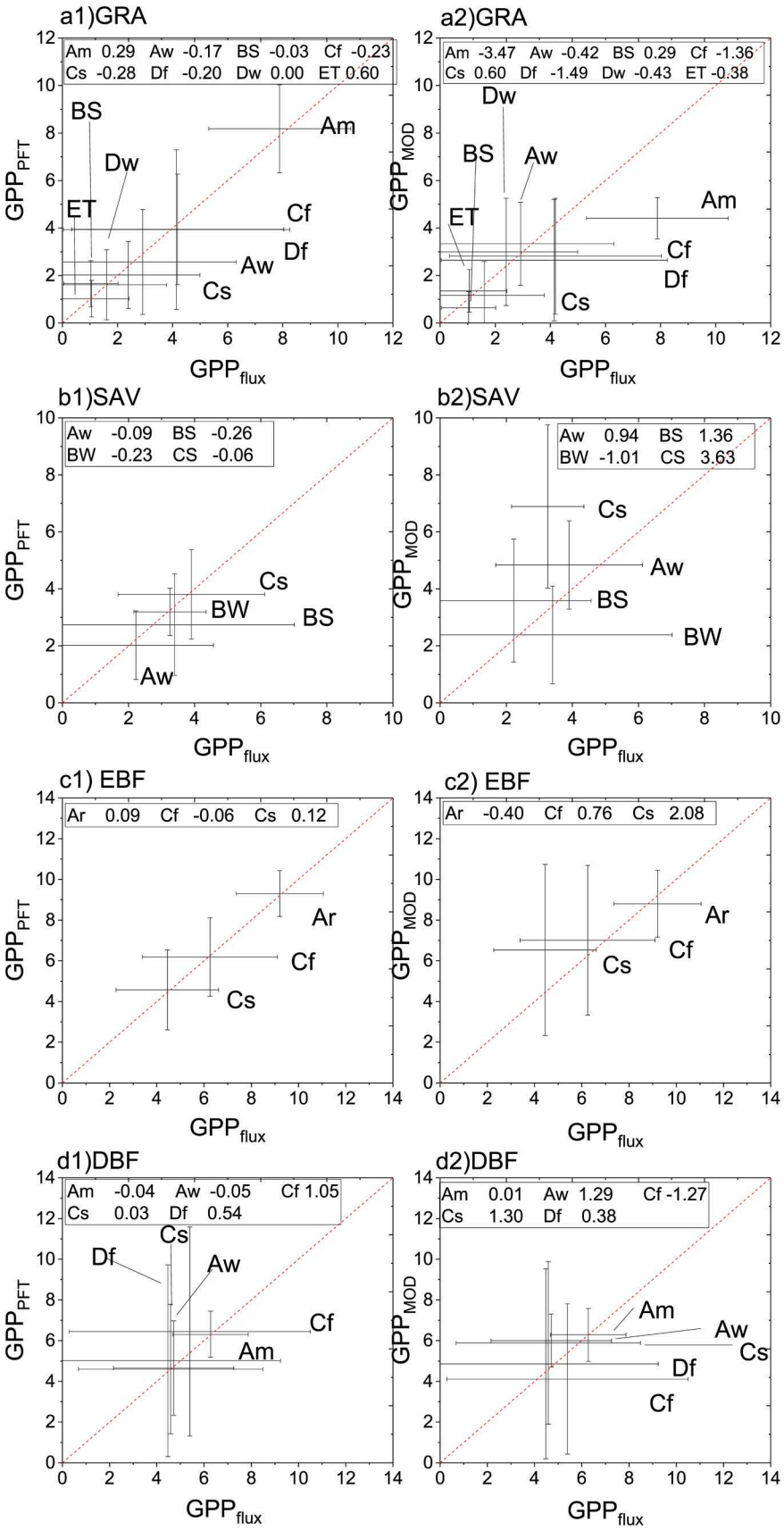

Fig. 8. Comparison of daily GPP between the climate-based GPP estimation method (PFT) and the MOD method, which does not take into account climate zone differences, against tower based GPP (flux). The error bar of each series is the intra-annual variance of GPP. The red dashed line in each subfigure is the 1:1 line. The units of the GPP data in are g C m^2 day^{-1}. (For interpretation of the references to colour in this figure legend, the reader is referred to the web version of this article.)

The interrelationship of temperature and VPD affects the scalar to $GPP_{POT,PFT}$. Under natural conditions, temperature and VPD are highly correlated (Fig. 5). Fig. 6b,d shows that the optimal temperature is less than 10 °C. This is because EBF_Cf and SAV_Cs reach their GPP_{POT} when VPD is low; however, when the VPD is low, the temperature is also lower. This caused the fitted optimal temperature of these PFTs to be less than 10 °C.It also affected the water scalar. Fig. 6f ~ h show that the water scalar is not 1 when VPD equals to 0. When the VPD equals to 0, it means that the temperature tends to be low. At this time, the temperature stress to GPP tends to be high. Thus, the VPD scalar is less than 1. Thus, separating the individual stresses of temperature and VPD needs to be improved.

4.3. Intercomparison to other GPP models

GPP_{PFT}, which has higher R^2 and lower RMSE than other GPP models, explained at least 4% more of GPP variance than other models (Fig. 7). Both GPP_{PFT} and GPP_{BESS}, incorporating plant trait differences, especially the $GPP_{POT,PFT}$ (in GPP_{PFT}) and Vcmax (in GPP_{BESS}) difference across PFTs, have high R^2 and RMSE for GPP estimation for each vegetation type. Compared to the GPP_{MOD} and GPP_{VPM} which use a constant LUE_{max} across vegetation types, GPP_{PFT} assumes that plant traits are very different across climate zones. With this improvement, the $GPP_{POT,PFT}$ corrected GPP_{max} across PFTs, the GPP_{PFT} model adjusted the range of GPP in different PFTs (Fig. 8). The plant trait was very different in EBF forests; however, the GPP_{MOD} assumed a constant canopy scale LUE_{max}, which was parameterized from the tropical EBF, represented for the different climate zones. The GPP_{PFT} assumed a different $GPP_{POT,PFT}$ across PFTs even in the same vegetation type. Thus, it reduced the mean bias of GPP estimation of GPP_{MOD} in temperate monsoon and Mediterranean climate zones. Similarly, it also reduced the GPP estimation uncertainties compared to GPP_{MOD} in tropical savannah, arid, and Mediterranean climate zones (Table 3). Thus, considering plant trait difference across PFTs improves the GPP estimation.

Unlike other selected models in this study, which assume that temperature and water stress is the same for all vegetation types across climate zones (Running et al., 2004; Xiao et al., 2004), the GPP_{PFT} model takes into account the climate stress and the plant trait differences across climate zones of the same vegetation type. Both considering the dominant climatic control factor between temperature and VPD, and the climate stress level across PFTs under various climatic conditions, provides a better representation of the climate stress for estimating GPP across PFTs (Fig. 6, Table 2). For example, GPP_{PFT} results in a lower RMSE than GPP_{MOD} for grassland. GPP_{PFT} identifies VPD as the dominant control factor in grasslands of tropical and Mediterranean climate zones (Seneweera et al., 1998), and temperature in grasslands of temperate, boreal, polar climate zone (Wingler et al., 2016). This sensitivity improves tracking climate stressors to GPP change. GPP_{BESS} and GPP_{VPM} perform better than GPP_{MOD}, but still assume that the climate stress is the same across PFTs, which has higher uncertainties than GPP_{PFT} in natural vegetation types.

4.4. Further improvements and applications

For future applications of this study, there are some aspects that need to be addressed. Firstly, GPP_{PFT} agrees less with GPP_{flux} than GPP_{BESS} in grassland areas. One explanation is that some GPP models such as GPP_{BESS} and GPP_{VPM} differentiate between C3 and C4 vegetation types (Table 3), which have different photosynthetic pathways, photosynthetic capacity and stress response to water content (Ito and Inatomi, 2012; Yan et al., 2015). Future improvements to the GPP_{PFT} model should also consider the differences in plant traits and climatic stressors of C3 and C4 species. Secondly, as the LUEmax in this study is based on canopy observations, (Zhang et al., 2018) have demonstrated that chlorophyll-scale LUE_{max} tends to be constant across C3 species. The red edge reflectance provides the insight for estimating chlorophyll-scale based LUE_{max} and GPP_{POT} (Lin et al., 2019) without specific PFT-based $GPP_{POT,PFT}$. Yet, the $GPP_{POT,PFT}$ could be used in the model with a specific PFT input. Lastly, as this study just focused on the modeling of natural vegetation types, there may be different growth rules for croplands and other artificial PFTs. Thus, these kinds of vegetation growth processes still need to be explored for global GPP mapping and carbon assessments.

5. Conclusions

PFTs derived from combining a simplified global vegetation distribution with climate zones, represent similar groups of plant species. This study suggested an improved framework of remote sensing data driven GPP estimation by incorporating both plant traits and dominant climatic control factors in various PFTs. In this study, the improved model is more accurate than the selected model. There were strong differences in maximum potential GPP (plant trait of photosynthesis) in different climate zones even when these had the same vegetation type, the same phenological period and incident energy. The dominant climate control factor also showed a high variance depending on the climate zones. Even under the same climate conditions, GPP stress varied across PFTs. The GPP estimated by the improved model that considered the differences in plant traits and dominant climatic forcing factors showed the highest agreement with carbon flux tower-based GPP. The results suggest that this framework of GPP estimation may reduce the uncertainties in terrestrial carbon evaluations in natural PFTs. Further global-scale GPP evaluations should consider plant trait differences in the modeling framework.

CRediT authorship contribution statement

Shangrong Lin: Writing - original draft, Writing - review & editing, Conceptualization, Methodology. **Jing Li:** Writing - original draft, Writing - review & editing, Funding acquisition, Project administration. **Qinhuo Liu:** Funding acquisition, Project administration, Supervision. **Beniamino Gioli:** Writing - original draft, Resources, Writing - original draft, Resources. **Eugenie Paul-Limoges:** Writing - original draft, Resources, Writing - original draft, Resources. **Nina Buchmann:** Writing - original draft, Resources. **Mana Gharun:** Writing - original draft, Resources. **Lukas Hörtnagl:** Writing - original draft, Resources. **Lenka Foltýnová:** Writing - original draft, Resources, Writing - original draft, Resources. **Jiri Dušek:** Writing - original draft, Resources. **Longhui Li:** Writing - original draft. **Wenping Yuan:** Writing - original draft, Writing - review & editing, Supervision.

Declaration of Competing Interest

The authors declare that they have no known competing financial interests or personal relationships that could have appeared to influence the work reported in this paper.

Acknowledgements

This work was supported by National Key Research and Development Program (2018YFA0605503), GF6 Project under Grant 30-Y20A03-9003-17/18. This work used eddy covariance data acquired and shared by the FLUXNET community, including these networks: AmeriFlux, AfriFlux, AsiaFlux, CarboAfrica, CarboEuropeIP, CarboItaly, CarboMont, ChinaFlux, Fluxnet-Canada, GreenGrass, ICOS, KoFlux, LBA, NECC, OzFlux-TERN, Swiss FluxNet, TCOS-Siberia, and USCCC. The ERA-Interim reanalysis data are provided by ECMWF and processed by LSCE. The FLUXNET eddy covariance data processing and harmonization was carried out by the European Fluxes Database Cluster, AmeriFlux Management Project, and Fluxdata project of FLUXNET, with the support of CDIAC and ICOS Ecosystem Thematic Center, and the

OzFlux, ChinaFlux and AsiaFlux offices. MG acknowledges funding by Swiss National Science Foundation project ICOS-CH Phase 2 20FI20_173691. This work was also supported by the Ministry of Education, Youth and Sports of the Czech Republic within the National Sustainability Programme I (NPU I), grant number LO1415 and by the project for national infrastructure support CzeCOS/ICOS Reg.No. LM2015061.

Appendix A. Supplementary material

Supplementary data to this article can be found online at https://doi.org/10.1016/j.jag.2021.102328.

References

Ali, A.A., et al., 2015. Global-scale environmental control of plant photosynthetic capacity. Ecol. Appl. 25 (8), 2349–2365. https://doi.org/10.1890/14-2111.1.
Baldocchi, D., et al., 2001. FLUXNET: A new tool to study the temporal and spatial variability of ecosystem-scale carbon dioxide, water vapor, and energy flux densities. Bull. Am. Meteorol. Soc. 82 (11), 2415–2434.
Beer, C., et al., 2010. Terrestrial gross carbon dioxide uptake: global distribution and covariation with climate. Science 329 (5993), 834–838.
Bernacchi, C.J., et al., 2002. Temperature response of mesophyll conductance. Implications for the determination of Rubisco enzyme kinetics and for limitations to photosynthesis in vivo. Plant Physiol. 130 (4), 1992–1998. https://doi.org/10.1104/pp.008250.water.
Bonan, G.B., et al., 2015. Reconciling leaf physiological traits and canopy flux data: Use of the TRY and FLUXNET databases in the Community Land Model version 4. J. Geophys. Res. Biogeosci. 117 (G2), 313–325.
Brando, P.M., et al., 2010. 'Seasonal and interannual variability of climate and vegetation indices across the Amazon', Proc. Natl. Acad. Sci. U. S. A., 107(33), pp. 14685–14690. doi: 10.1073/pnas.0908741107.
Chen, J.M., et al., 1999. Daily canopy photosynthesis model through temporal and spatial scaling for remote sensing applications. Ecol. Model. 124 (2–3), 99–119.
Dass, P., et al., 2015. Environmental controls on the greening of terrestrial vegetation across northern Eurasia. Biogeosci. Discuss. 12 (12), 9121–9162. https://doi.org/10.5194/bgd-12-9121-2015.
Farquhar, G.D., von Caemmerer, S., Berry, J.A., 1980. A biochemical model of photosynthetic CO2 assimilation in leaves of C3 species. Planta 149 (1), 78–90. https://doi.org/10.1007/BF00386231.
Flexas, J., et al., 2014. Photosynthetic limitations in Mediterranean plants: A review. Environ. Exp. Bot. 103, 12–23. https://doi.org/10.1016/j.envexpbot.2013.09.002.
Garbulsky, M.F., et al., 2014. Photosynthetic light use efficiency from satellite sensors: From global to Mediterranean vegetation. Environ. Exp. Bot. 103, 3–11. https://doi.org/10.1016/j.envexpbot.2013.10.009.
Gebremichael, M., Barros, A.P., 2006. Evaluation of MODIS Gross Primary Productivity (GPP) in tropical monsoon regions. Remote Sens. Environ. 100 (2), 150–166. https://doi.org/10.1016/j.rse.2005.10.009.
Goward, S.N., Tucker, C.J., Dye, D.G., 1985. North American vegetation patterns observed with the NOAA-7 advanced very high resolution radiometer. Vegetatio 64 (1), 3–14.
Groenendijk, M., Dolman, A.J., van der Molen, M.K., et al., 2011. Assessing parameter variability in a photosynthesis model within and between plant functional types using global Fluxnet eddy covariance data. Agric. For. Meteorol. 151 (1), 22–38. https://doi.org/10.1016/j.agrformet.2010.08.013.
Grossiord, C., Sevanto, S., Limousin, J., et al., 2017a. Manipulative experiments demonstrate how long-term soil moisture changes alter controls of plant water use. Environ. Exp. Bot. 152, 19–27.
Grossiord, C., Sevanto, S., Adams, H.D., et al., 2017b. Precipitation, not air temperature, drives functional responses of trees in semi-arid ecosystems. J. Ecol. 105 (1), 163–175.
Grossiord, C., et al., 2020. 'Tansley review Plant responses to rising vapor pressure deficit'. doi: 10.1111/nph.16485.
Harper, A.B., et al., 2016. Improved representation of plant functional types and physiology in the Joint UK Land Environment Simulator (JULES v4.2) using plant trait information. Geosci. Model Dev. 9 (7), 2415–2440. https://doi.org/10.5194/gmd-9-2415-2016.
He, L., et al., 2018. Changes in the shadow: the shifting role of shaded leaves in global carbon and water cycles under climate change. Geophys. Res. Lett. 45 (10), 5052–5061. https://doi.org/10.1029/2018GL077560.
Ide, R., Nakaji, T., Oguma, H., 2010. Assessment of canopy photosynthetic capacity and estimation of GPP by using spectral vegetation indices and the light-response function in a larch forest. Agric. For. Meteorol. 150 (3), 389–398. https://doi.org/10.1016/j.agrformet.2009.12.009.
Ito, A., Inatomi, M., 2012. Use of a process-based model for assessing the methane budgets of global terrestrial ecosystems and evaluation of uncertainty. Biogeosciences 9 (2), 759–773. https://doi.org/10.5194/bg-9-759-2012.
Jarvis, P.G., 1976. Interpretation of variations in leaf water potential and stomatal conductance found in canopies in field. Philos. Trans. Royal Soc. B Biol. Sci. 273, 593–610.
Jiang, C., Ryu, Y., 2016. Multi-scale evaluation of global gross primary productivity and evapotranspiration products derived from Breathing Earth System Simulator (BESS). Remote Sens. Environ. 186, 528–547. https://doi.org/10.1016/j.rse.2016.08.030.
Joiner, J., et al., 2018. Estimation of terrestrial global gross primary production (gpp) with satellite data-driven models and eddy covariance flux data. Remote Sens. 10 (9), 1346.
Jung, M., et al., 2011. Global patterns of land-atmosphere fluxes of carbon dioxide, latent heat, and sensible heat derived from eddy covariance, satellite, and meteorological observations. J. Geophys. Res. Biogeosci. 116 (3), 1–16. https://doi.org/10.1029/2010JG001566.
Kanniah, K.D., Beringer, J., Hutley, L.B., 2013. 'Response of savanna gross primary productivity to interannual variability in rainfall: Results of a remote sensing based light use efficiency model'. doi: 10.1177/0309133313490006.
Kattge, J., et al., 2011. TRY - a global database of plant traits. Glob. Change Biol. 17 (9), 2905–2935. https://doi.org/10.1111/j.1365-2486.2011.02451.x.
Keenan, T.F., Williams, C.A., 2018. 'The Terrestrial Carbon Sink'.
Kumagai, T., et al., 2015. How do rubber (Hevea brasiliensis) plantations behave under seasonal water stress in northeastern Thailand and central Cambodia. Agric. For. Meteorol. 213, 10–22.
Lasslop, G., et al., 2010. Separation of net ecosystem exchange into assimilation and respiration using a light response curve approach: Critical issues and global evaluation. Glob. Change Biol. 16 (1), 187–208. https://doi.org/10.1111/j.1365-2486.2009.02041.x.
Lin, S., et al., 2019. Evaluating the effectiveness of using vegetation indices based on red-edge reflectance from Sentinel-2 to estimate gross primary productivity. Remote Sens. 11 (11) https://doi.org/10.3390/rs11111303.
Lin, X., et al., 2017. Seasonal fluctuations of photosynthetic parameters for light use efficiency models and the impacts on gross primary production estimation. Agric. For. Meteorol. 236, 22–35. https://doi.org/10.1016/j.agrformet.2016.12.019.
Liu, J., Ramba, S., Mouillot, F., 2015. Soil drought anomalies in MODIS GPP of a mediterranean broadleaved evergreen forest. Remote Sens. 7 (1), 1154–1180. https://doi.org/10.3390/rs70101154.
Luo, X., et al., 2019. 'Improved estimates of global terrestrial photosynthesis using information on leaf chlorophyll content', (February), pp. 2499–2514. doi: 10.1111/gcb.14624.
Madani, N., et al., 2017. Global analysis of bioclimatic controls on ecosystem productivity using satellite observations of solar-induced chlorophyll fluorescence. Remote Sens. 9 (6) https://doi.org/10.3390/rs9060530.
Musavi, T., et al., 2016. Potential and limitations of inferring ecosystem photosynthetic capacity from leaf functional traits. Ecol. Evol. 6 (20), 7352–7366. https://doi.org/10.1002/ece3.2479.
Nemani, R.R., et al., 2003. Climate-driven increases in global terrestrial net primary production from 1982 to 1999. Science 300 (5625), 1560–1563. https://doi.org/10.1126/science.1082750.
Niinemets, Ü., Keenan, T.F., Hallik, L., 2015. A worldwide analysis of within-canopy variations in leaf structural, chemical and physiological traits across plant functional types. New Phytol. 205 (3), 973–993. https://doi.org/10.1111/nph.13096.
Pappas, C., Fatichi, S., Burlando, P., 2016. Modeling terrestrial carbon and water dynamics across climatic gradients: Does plant trait diversity matter? New Phytol. 209 (1), 137–151. https://doi.org/10.1111/nph.13590.
Peel, M.C., et al., 2007. Updated world map of the Köppen-Geiger climate classification To cite this version : HAL Id : hal-00298818 Updated world map of the K oppen-Geiger climate classification. Hydrol. Earth Syst. Sci. 11 (5), 1633–1644.
Pereira, L.S., et al., 2015. Crop evapotranspiration estimation with FAO56: Past and future. Agric. Water Manag. 147, 4–20.
Piao, S., et al., 2011. Changes in satellite-derived vegetation growth trend in temperate and boreal Eurasia from 1982 to 2006. Glob. Change Biol. 17 (10), 3228–3239. https://doi.org/10.1111/j.1365-2486.2011.02419.x.
Reichstein, M., et al., 2014. 'Linking plant and ecosystem functional biogeography', Proc. Natl. Acad. Sci. U. S. A., 111(38), pp. 13697–13702. doi: 10.1073/pnas.1216065111.
Richardson, Andrew D., et al., 2007. Environmental variation is directly responsible for short- but not long-term variation in forest-atmosphere carbon exchange. Glob. Change Biol. 13 (4), 788–803. https://doi.org/10.1111/j.1365-2486.2007.01330.x.
Rogers, A., et al., 2017. A roadmap for improving the representation of photosynthesis in Earth system models. New Phytol. 213 (1), 22–42. https://doi.org/10.1111/nph.14283.
Running, S.W., et al., 2004. A continuous satellite-derived measure of global terrestrial primary production. Bioscience 54 (6), 547–560.
Ryu, Y., et al., 2011. Integration of MODIS land and atmosphere products with a coupled-process model to estimate gross primary productivity and evapotranspiration from 1 km to global scales. Global Biogeochem. Cycles 25 (4), 1–24. https://doi.org/10.1029/2011GB004053.
Ryu, Y., et al., 2018. 'MODIS-derived global land products of shortwave radiation and diffuse and total photosynthetically active radiation at 5 km resolution from 2000'. Remote Sens. Environ. 204, 812–825. https://doi.org/10.1016/j.rse.2017.09.021.
Ryu, Y., Berry, J.A., Baldocchi, D.D., 2019. What is global photosynthesis? History, uncertainties and opportunities', Remote Sens. Environ. 223, 95–114. https://doi.org/10.1016/j.rse.2019.01.016.
Schaefer, K., et al., 2012. A model-data comparison of gross primary productivity: Results from the north American carbon program site synthesis. J. Geophys. Res. Biogeosci. 117 (3), 1–15. https://doi.org/10.1029/2012JG001960.
Sendall, K.M., et al., 2015. Acclimation of photosynthetic temperature optima of temperate and boreal tree species in response to experimental forest warming. Glob. Change Biol. 21 (3), 1342–1357. https://doi.org/10.1111/gcb.12781.

Seneweera, S.P., et al., 1998. High vapour pressure deficit and low soil water availability enhance shoot growth responses of a C4 grass (Panicum coloratum cv. Bambatsi) to CO2 enrichment. Funct. Plant Biol. 25 (3), 287–292.
Sims, D.A., et al., 2008. A new model of gross primary productivity for North American ecosystems based solely on the enhanced vegetation index and land surface temperature from MODIS. Remote Sens. Environ. 112 (4), 1633–1646. https://doi.org/10.1016/j.rse.2007.08.004.
Sitch, S., et al., 2003. Evaluation of ecosystem dynamics, plant geography and terrestrial carbon cycling in the LPJ dynamic global vegetation model. Glob. Change Biol. 9 (2), 161–185. https://doi.org/10.1046/j.1365-2486.2003.00569.x.
Sjöström, M., et al., 2013. Evaluation of MODIS gross primary productivity for Africa using eddy covariance data. Remote Sens. Environ. 131, 275–286. https://doi.org/10.1016/j.rse.2012.12.023.
Slot, M., Winter, K., 2017. In situ temperature relationships of biochemical and stomatal controls of photosynthesis in four lowland tropical tree species. Plant, Cell Environ. 40 (12), 3055–3068. https://doi.org/10.1111/pce.13071.
Sun, Z., et al., 2019. Evaluating and comparing remote sensing terrestrial GPP models for their response to climate variability and CO 2 trends. Sci. Total Environ. 668, 696–713. https://doi.org/10.1016/j.scitotenv.2019.03.025.
Turner, D.P., et al., 2005. Site-level evaluation of satellite-based global terrestrial gross primary production and net primary production monitoring. Glob. Change Biol. 11 (4), 666–684. https://doi.org/10.1111/j.1365-2486.2005.00936.x.
Turner, D.P., et al., 2006. Evaluation of MODIS NPP and GPP products across multiple biomes. Remote Sens. Environ. 102 (3–4), 282–292. https://doi.org/10.1016/j.rse.2006.02.017.
Verbeeck, H., et al., 2008. Multi-year model analysis of GPP in a temperate beech forest in France. Ecol. Model. 210 (1), 85–103.
Wagle, P., et al., 2015. Biophysical controls on carbon and water vapor fluxes across a grassland climatic gradient in the United States. Agric. For. Meteorol. 214–215, 293–305. https://doi.org/10.1016/j.agrformet.2015.08.265.
Walker, A., et al., 2017. The impact of alternative trait-scaling hypotheses for the maximum photosynthetic carboxylation rate (vcmax) on global gross primary production. New Phytologist.
Wei, S., et al., 2017. A global study of GPP focusing on light-use efficiency in a random forest regression model. Ecosphere 8 (5). https://doi.org/10.1002/ecs2.1724.
Wingler, A., Hennessy, D., Parsons, A.J., 2016. 'Limitation of grassland productivity by low temperature and seasonality of growth', 7(July), pp. 1–6. doi: 10.3389/fpls.2016.01130.
Wu, C., Niu, Z., Gao, S., 2010. Gross primary production estimation from MODIS data with vegetation index and photosynthetically active radiation in maize. J. Geophys. Res. Atmos. 115 (12), 1–11. https://doi.org/10.1029/2009JD013023.
Wu, J., et al., 2017a. Partitioning controls on Amazon forest photosynthesis between environmental and biotic factors at hourly to interannual timescales. Glob. Change Biol. 23 (3), 1240–1257. https://doi.org/10.1111/gcb.13509.
Wu, Z., et al., 2017b. Climate data induced uncertainty in model-based estimations of terrestrial primary productivity. Environ. Res. Lett. 12 (6), 64013. https://doi.org/10.1088/1748-9326/aa6fd8.
Xiao, X., Zhang, Q., et al., 2004a. Modeling seasonal dynamics of gross primary production of an evergreen needleleaf forest using MODIS images and climate data. Simulation 15 (603), 1–49.
Xiao, J., et al., 2019. Remote sensing of the terrestrial carbon cycle: A review of advances over 50 years. Remote Sens. Environ. 233 (August), 111383 https://doi.org/10.1016/j.rse.2019.111383.
Xiao, X., Hollinger, D., et al., 2004b. Satellite-based modeling of gross primary production in an evergreen needleleaf forest. Remote Sens. Environ. 89 (4), 519–534. https://doi.org/10.1016/j.rse.2003.11.008.
Xiao, Z., et al., 2015. Estimating the fraction of absorbed photosynthetically active radiation from the MODIS data based GLASS leaf area index product. Remote Sens. Environ. 171, 105–117. https://doi.org/10.1016/j.rse.2015.10.016.
Yan, H., et al., 2015. Improved global simulations of gross primary product based on a new definition of water stress factor and a separate treatment of C3 and C4 plants. Ecol. Model. 297, 42–59. https://doi.org/10.1016/j.ecolmodel.2014.11.002.
Yuan, W., et al., 2007. Deriving a light use efficiency model from eddy covariance flux data for predicting daily gross primary production across biomes. Agric. For. Meteorol. 143 (3–4), 189–207.
Yuan, W., Cai, W., Xia, J., Chen, J., Liu, S., Dong, W., Merbold, L., Law, B.E., et al., 2014. Global comparison of light use efficiency models for simulating terrestrial vegetation gross primary production based on the LaThuile database. Agric. For. Meteorol. 192, 108–120.
Zhang, Y., et al., 2017. A global moderate resolution dataset of gross primary production of vegetation for 2000–2016. Sci. Data 4, 170165. https://doi.org/10.1038/sdata.2017.165.
Zhang, Y., Xiao, X., Wolf, S., Wu, J., Wu, X., 2018 'Spatio-temporal convergence of maximum daily light-use efficiency based on radiation absorption by canopy chlorophyll', pp. 3508–3519. doi: 10.1029/2017GL076354.
Zhang, Y., et al., 2016. Consistency between sun-induced chlorophyll fluorescence and gross primary production of vegetation in North America. Remote Sens. Environ. 183, 154–169. https://doi.org/10.1016/j.rse.2016.05.015.